RSC Advances

This is an *Accepted Manuscript*, which has been through the Royal Society of Chemistry peer review process and has been accepted for publication.

Accepted Manuscripts are published online shortly after acceptance, before technical editing, formatting and proof reading. Using this free service, authors can make their results available to the community, in citable form, before we publish the edited article. This *Accepted Manuscript* will be replaced by the edited, formatted and paginated article as soon as this is available.

You can find more information about *Accepted Manuscripts* in the Information for Authors.

Please note that technical editing may introduce minor changes to the text and/or graphics, which may alter content. The journal's standard Terms & Conditions and the Ethical guidelines still apply. In no event shall the Royal Society of Chemistry be held responsible for any errors or omissions in this *Accepted Manuscript* or any consequences arising from the use of any information it contains.

ROYAL SOCIETY OF CHEMISTRY

www.rsc.org/advances

Synthesis of Fluorinated SnO_2 3D Hierarchical Structure Assembled from Nanosheets and Its Enhanced Photocatalytic Activity

Youzhi Wang, Guoe Cheng, Yu Zhang, Hanzhong Ke and Chunling Zhu*

Faculty of Material & Chemistry

China University of Geosciences

Wuhan, 430074, P.R. China

**E-mail: chengguoe68@aliyun.com, chengge@cug.edu.cn*

Abstract

The fluorinated SnO_2 3D hierarchical structures assembled from nanosheets were synthesized via a hydrothermal treatment of stannous fluoride in the presence of appropriate amount of adipic acid. The as-prepared products were characterized in detail by FESEM/TEM/XRD/BET/XPS/UV-vis DRS techniques. The SnO_2 nanosheets with tetragonal rutile structure were single-crystalline nature and the exposed planes should be $\{1\bar{1}1\}$ facets. A small amount of fluorine ions were observed to be adsorbed on the surface of SnO_2 physically. It was found that both of F^- and adipic acid played important roles in the formation of SnO_2 nanostructures. The as-prepared product presented excellent photocatalytic degradation of RhB which reached 100 % within 20 min under UV light irradiation.

Key words: SnO_2; nanosheets; fluorinated; photocatalysis

1. Introduction

As a type of important functional inorganic materials, tin dioxide (SnO_2), a wide band gap semiconductor (3.6 eV) with rutile-type crystal structure, has aroused widespread concern because of its wide applications in chemical sensors, lithium-ion batteries, solar cells, *etc*.[1-6] However, recent researches revealed that SnO_2 nanostructures also show reasonable photocatalytic activities.[7-11]Because the properties of metal oxide materials strongly depend on their shape and microstructure, efforts have been focused on the synthesis of novel nanostructures with tailored morphology to improve the photocatalytic performance of SnO_2. Hao *et al.* [7] prepared SnO_2 nanoparticles with small size through a hydrothermal route, which showed reasonable photocatalytic towards degradation of Rhodamine B (RhB) dye. Li *et al.* [9] reported that V-shaped SnO_2 nanorods prepared by a solvothermal method showed unprecedented visible-light-driven photocatalytic activities. Wang *et al*. [11] obtained hollow SnO_2 microspheres by a carbon-template hydrothermal method also showed remarkable photocatalytic activities for degradation of RhB dye. Recently, 2D non-layered semiconductor nanosheets with a large lateral size and a small thickness, have recently attracted considerable attention owing to their unique electronic, optical and surface properties.[12-16] In general, their nanoscale thickness could not only represent an ultrahigh surface atom percentage with great efficient active sites and specific facet exposed outside but also allows for prompt migration of the photogenerated charge carriers to the surface, thus the photocatalytic activity could be greatly improved.[12-14] Additionally, ultrathin nanosheets structure with high surface areas can adsorb more target molecules and incident light, thus benefits the photocatalysis happened on the surface of them.[15] Furthermore, due to their low anisotropy, these 2D nanosheets could be easily grown or self-assembled into 3D hierarchical structures.[6,16] Which could exhibit the advantages of the pristine 2D nanosheets building blocks, and more importantly, also possess new physicochemical properties arising from their secondary

RSC Advances Accepted Manuscript

architecture. Despite these advantages, few researches about the synthesis and application of 2D ultrathin SnO_2 nanosheets were reported. Wang *et al*. [2] reported the fabrication and excellent gas sensing properties of SnO_2 flower-like hierarchical structures assembled by 2D nanosheets. Zhu *et al.* [6] prepared 2D ultrathin SnO_2 nanosheets through microwave-assisted solution-phase growth. These graphene-like nanosheets with a thickness of 2~3 nm delivered remarkably enhanced lithium storage performances over their counterparts. Recently, Liu's group[8] synthesized a novel 3D hierarchical structures assembled by 2D nanosheets through a simple hydrothermal approach. It was found that this sample not only showed superior performance when applied in gas sensing and supercapacitor but also presented amazing photocatalytic activities towards degradation of organic dyes when used as photocatalyst. Hence, the fabrication of 2D ultrathin SnO_2 nanostructure would be highly desirable for application as advanced photocatalyst.

On one other hand, it has been revealed that F ions can modified the TiO_2 crystal growth with shape, exposed facets controlled.[17-21] Yang *et al.* [17] firstly revealed that the F-mediated crystal synthesis can lead to a growth of TiO_2 crystals with shape controlled and 47% {001} facets exposed. Inspired by this pioneering work, many similar researches were aroused subsequently.[18-21] Not limited to TiO_2, it was recently found that the fluorine ions can also greatly influence the morphologies of SnO_2 nanocrystals. Chen *et al.* [22] found that the NH_4F additive plays an important role in determining the sheet-like morphology of the obtained product. Wang *et al.* [2] also revealed that the growth orientation of their fabricated 2D SnO_2 nanosheets can be controlled by adjusting the ratio of fluorine to tin precursor. Furthermore, it is also demonstrated that fluorination of semiconductor photocatalysts, involving either fluoride adsorption or lattice fluorine-doping, can significantly modify the bulk and surface characteristics and thus greatly benefit the photocatalysis.[18, 23-25] Hu and co-workers reported that the surface fluorinated ultrathin TiO_2 nanosheet superstructures showed a much enhanced photocatalytic activity towards the degradation of RhB dye while compared with commercial P25 for the inhibited electron/hole (e/h+) recombination.[23] Yang et al. [18] prepared TiO_2 nanosheets with the synthesis mediated by HF and found that the sample can achieve superior photoreactivity (more than 5 times) compared to P25 because of generation of more $^{\cdot}OH$ free radicals on the surface of those surface fluorinated nanosheets. Note that the progress have been made in TiO_2 photocatalysis, it can be expected that the introduction of fluorine ions into the synthesis system of SnO_2 nanocrystal also bring some improvements of photocatalytic activities. Actually, our recent research had revealed that when introducing F ions into the synthesis system, the obtained SnO_2 particles with surface fluorinated showed significantly enhanced photocatalytic activity for degradation of RhB dye.[7]

Herein, we report a facile hydrothermal method for synthesis of SnO_2 hierarchical structure assembled from surface fluorinated ultrathin SnO_2 nanosheets. The morphological, structural and compositional, as well as the formation mechanism of obtained samples were investigated. Moreover, the photocatalytic activity test shows that the obtained SnO_2 hierarchical structure exhibits an excellent photocatalytic activity for degradation of RhB dye under a 300W high-pressure mercury lamp irradiation at room temperature.

2. Experimental

2.1 Sample preparation

The SnO_2 nanaostructures were synthesized by a facile hydrothermal method. In a typical preparation procedure, 3 mmol of stannous fluoride (SnF_2) and 6 mmol of adipic acid were dissolved into 50 ml of aqueous solution under vigorous stirring for 30 min. The obtained

RSC Advances Accepted Manuscript

transparent clear solution was transferred to a Teflon-covered stainless steel autoclave and then heated in an electronic oven at 180°C for 6 h. After the autoclave was cooled down to room temperature naturally, the precipitates were collected by centrifugation, washed several times with distilled water and absolute ethanol, and then dried at 60°C for 24 h. The as-obtained product was denoted as **SA-6**.

2.2 **Characterization**

The microscopic nanostructures of the as-prepared samples were observed by transmission electron microscopy (TEM; FEI Tecnai G^2 20 operated at 200 kV), field emission scanning electron microscopy (FESEM, quanta-200 operated at 25 kV) and high-resolution transmission electron microscopy (HRTEM; Tecnai G^2 20 U-TWIN operated at 200 kV). Surface chemical analysis of the samples was conducted on an X-ray photoelectron spectroscope (XPS, Multilab 2000). All binding energies were referenced to the C 1s peak with a binding energy of 284.7 eV of the surface adventitious carbon. The crystallite structures of the materials were investigated by analyzing the X-ray powder diffraction (XRD, Bruker Axs D8-Focus, Cu Kα radiation with λ = 1.5406 Å). The specific surface area and pore size distribution were characterized by analyzing the N_2 adsorption and desorption isotherms using Micrometrics ASAP 2000 equipment. The optical absorption properties of samples was detected by UV-vis diffuse reflectance spectra (UV-vis DRS, UV-2550) in the range of 240-850 nm. The existence of hydroxyl radicals was investigated by the photoluminescence-terephthalic acid (PL-TA) technique. The photoluminescence spectra of generated 2-hydroxyterephthalic acid were recorded on a Hitachi F-4500 fluorescence spectrophotometer.

2.3 **Evaluation of photocatalytic activity**

The photocatalytic activities were tested by photochemical reactions instrument (BL-GHX-IV) and UV–vis adsorption spectra (UV-1801). RhB was used as a probe molecule to research the photocatalytic activities of the hollow SnO_2 nanospheres. Typically, 50 mg of catalysts were dispersed in 50 mL of 10 mg/L RhB aqueous solution in a quartz tube. Prior to irradiation, the suspension was magnetically stirred for one hour in the dark to favor the adsorption-desorption equilibration. Subsequently, the suspension was irradiated under a 300 W high-pressure mercury lamp. During illumination, about 5 mL of the above solution was taken out at an interval of 10 min and centrifuged for UV-vis analysis.

3. Results and discussion

The crystalline phase of the sample **SA-6** was confirmed by XRD. As shown in Fig. 1, all the diffraction peaks can be indexed to the rutile phase SnO_2 (cassiterite, JCPDS card No. 41-1445, space group: $P4_2/mnm$) with tetragonal lattice constant a=4.738 Å and c=3.187 Å. No other crystallographic phase can be detected. The relatively broader diffraction peaks are believed to result from the small crystallite size. The relative intensities of the peaks deviate from those of the bulk material, suggesting the anisotropic growth of the SnO_2 crystals.

The morphology and microstructure of the sample **SA-6** were further investigated by FESEM, TEM and HRTEM. The FESEM image (Fig. 2a, b) show that the sample **SA-6** consists of many two-dimensional nanosheets which are connected to each other to build flowerlike hierarchical structures. The shape of a single hierarchical structure is irregular and its size varies from hundreds nanometers to several micrometers. Fascinatingly, it can be seen that the nanosheets with smooth and clean surfaces aren't entirely flat but slightly curly and arranged to point out from the center. This scrolled nature of this sort of structure can be ascribed to the minimization of surface

RSC Advances Accepted Manuscript

energy. Further, the thickness of the nanosheets was measured to be only ~6 nm from the FESEM image. A TEM image of a single flowerlike hierarchical structure is shown in Fig. 2c. The size and morphology are consistent with the observation from the FESEM images. The HRTEM image exhibits the well defined lattice fringes with the lattice spacing of 0.337 and 0.265 nm(Figure 2d), which correspond to the (110) and $(\bar{1}01)$ lattice planes of SnO_2, respectively. Many structural defects can be obviously observed in the SnO_2 nanosheets. Inset in Figure 2d exhibits its FFT pattern showing the observation is along the $(1\bar{1}1)$ projection. Considering the crystallographic structure of SnO_2, it might be deduced that the nominal exposed top and bottom planes of these nanosheets should be $\{1\bar{1}1\}$ facets, which is in agreement with that observed in a previous report.[16]

To evaluate the pore structure and pore sizes of the sample **SA-6**, the N_2 adsorption–desorption isotherms was investigated, as shown in Fig. 3. The isotherms of the samples is of classical type IV with a H3 hysteresis between the adsorption and desorption curves, indicating the presence of mesoporous in the materials, which are formed by the aggregation of sheet-like or plate-like particles. The pore size distribution curve determined by the Barrett–Joyner–Halenda (BJH) method from desorption branch of a nitrogen isotherm is shown in Fig.3 (inset). It shows a narrow pore size distribution of ~4 nm. The surface area is found to be 61.5m^2/g.

XPS measurements were carried out to investigate the chemical compositions and the existence forms of elements in the sample. Fig. 4 presents the XPS spectrum of the as-prepared SnO_2 sample. The spectrum clearly indicates the signature photo-electron peaks of Sn, O, C and F without the presence of any other impurities (Fig. 4a). The C element could be attributed to the adventitious carbon-based contaminant.[26] The double spectral lines of Sn 3d are seen at the binding energy of 486.5 eV (Sn $3d_{5/2}$) and 494.9 eV (Sn $3d_{3/2}$) with a spin-orbit splitting of 8.4 eV(Fig. 4b), which is in agreement with the reported value in the literature.[2, 27] The Sn $3d_{5/2}$ region shows a single peak at a binding energy of 486.5 eV, indicating that the sample was composed of only the Sn(IV) state, and with no noticeable Sn(II), which is expected at 485.8 eV, nor Sn(0), which is at 484.5 eV.[28] High resolution XPS spectra of O 1s are shown in Figure 4c. As seen from the spectrum, the O 1s spectrum is decomposed into two Gaussian curves after removal of the background. The peaks appearing at 530.6 eV and 531.8 eV are attributed to crystal lattice oxygen (Sn-O) and hydroxyl.[29] The F 1s binding energy peak at 684 eV is attributed to the fluorine ions physically adsorbed on the surface of SnO_2 (Fig. 4d). The surface fluoride (Sn-F) could be formed by ligand exchange reaction between F surface hydroxyl groups.[24,30] No signal of F^- in the lattice of SnO_2（688.5 eV）is found.[31] Actually, it has been demonstrated that the surface fluorination of TiO_2 readily takes place at an acidic hydrothermal environment, which prevents lattice substitution of F^- for O^{2-}.[24, 32]

Both of the F^- and adipic acid were proved to play an important role in the formation of SnO_2 hierarchical nanostructures. Control experiments have shown that, without adipic acid or using $SnCl_2$ instead of SnF_2 (corresponding products were denote as Sn, SA-Cl respectively), some impure peaks (marked with*) are found to exist in SnO_2 nanocrystals (Fig. S1a(supplementary information)). The morphologies of the products aren't SnO_2 nanosheet hierarchical structure but nanospheres (Fig. S1b, c). Otherwise, various dosages (1mmol, 3mmol, 9mmol) of adipic acid were introduced in the hydrothermal system (the corresponding products were denoted as SA-1, SA-3 and SA-9 respectively) to examine the effects on the as-prepared SnO_2 structures. As can be seen from the FESEM images shown in Fig. 2S (supplementary information), the samples are all composed of SnO_2 nanosheet hierarchical nanostructures (Fig. 2S(a-d)). With the dosage of adipic

RSC Advances Accepted Manuscript

acid increased, the nanosheets slightly became thinner and the gaps among the nanosheets became larger. Furthermore, the XRD patterns of these samples reveal that the widths of the diffraction peaks became narrower steadily with the dosage of adipic acid increased (Fig. S2e), indicating that the introduction of adipic acid could improve crystallinity of SnO_2 nanoparticles. However, with the dosage increased to 9mmol, some impure peaks (marked with*) are found to exist in SnO_2 nanocrystals.

Fig. 5 present the TEM images and XRD patterns of the sample **SA-6** collected at different hydrothermal time during the formation of SnO_2 nanosheet hierarchical structures. It can be seen that tiny SnO_2 nanoparticles were formed within 10min of hydrothermal process and self-assembly oriented to flake gatherings. After 30min of reaction, numerous mini-nanosheets were formed and the gaps among these nanoparticles could be observed obviously, which characterized as localized dissolution and recrystallization. When the reaction time was 3h, the oriented crystal growth of SnO_2 nanosheets appeared more apparently. Many 2D SnO_2 nanosheets extended fast and the small nanoparticle were further consumed. As the hydrothermal process was prolonged to 6h, high yield and uniform hierarchical SnO_2 nanostructures were produced. The XRD patterns showed that the rutile phase SnO_2 formed within only 10 min of reaction and the crystallinities of these intermediates were gradually improved with the hydrothermal process prolonged.

The formation of SnO_2 from SnF_2 can be illustrated as follows[33]

(1) $2Sn^{2+} + O_2 + 4H^+ \rightarrow 2Sn^{4+} + 2H_2O$

(2) $Sn^{4+} + 4H_2O \rightarrow Sn(OH)_4 + 4H^+$

(3) $Sn(OH)_4 \rightarrow SnO_2 + 2H_2O$

The introduction of adipic acid could adjust the pH of the solution to 4-5. In addition, as a chelating ligand with a strong coordinating ability, adipic acid can coordinate with tin ions (Sn^{4+}) and the formation of the complexes can sharply reduce the availability of free tin ions in aqueous solution, resulting in a slow reaction rate. That is important for the formation of an oriented crystal growth. Generally, during the crystal growth processes under equilibrium conditions, the high-energy facets diminish quickly and the crystal spontaneously evolves into specific shape with exposed facets that minimize the total surface free energy.[34] Wu *et al.*[16] also synthesize the similar SnO_2 nanostructures using tin(II) chloride dehydrate as the tin source. They found that the hydrolysis of tin(II) could result in some sheet-like intermediates, and the formation of SnO_2 nanostructures are based on the oxidation of these sheet-like intermediates as structure-directing precursors. However, no obvious phase related to SnO was detected in our primary intermediates after 10min of hydrothermal process. On the other hand, it has been demonstrated that selective adsorption of fluorine ions on the anatase TiO_2 high energy facets can enhance its relative stability by modifying and reducing the surface energy during the crystal growth, and finally lead to high energy facets exposed.[34] Recently, it was found that the fluorine ions could also be used as the morphology controlling agent which greatly influenced the morphologies of SnO_2 nanocrystals.[2,22] Wang *et al.* further revealed through first principles density functional theory (DFT) calculations, the fluoride capping lowered the surface energies of the facets significantly in different degree.[2] They successfully synthesized hierarchical nanoflowers assembled from SnO_2 nanosheets with high-index $(11\bar{3})$ and $(10\bar{2})$ facets exposed by adjusting the ratio of fluorine to tin precursor ($R_{F/Sn}$) from 3.0 to 4.8. Here, we obtained ultrathin SnO_2 nanosheets with $\{1\bar{1}1\}$ exposed by using

RSC Advances Accepted Manuscript

SnF_2 as both of the fluorine to tin precursor. So we take the idea that the formation of the as-obtained nanostructures should be mainly resulted from joint efforts the adipic acid and F^-.

The UV-vis DRS of SA-6 is presented in Fig. 3S (supplementary information) to detect its optical absorption properties and the information of its band gap. It can be seen that the sample SA-6 has a strong absorption in the UV region, which agrees with previous reports.[7] Interestingly, the absorption of the sample is observed to extent to visible region. The band gap related to direct allowed transition was estimated to be ca. 2.9 eV based on the intercept of the tangent of the plots of $(ahv)^2$ versus hν, which is much smaller than that of bulk SnO_2, usually 3.6 eV. It is reported that the surface fluorination of photocatalyst could not enhance the visible light absorption of photocatalyst.[24] So this result may be ascribed to the structure defects of SA-6.

Fig. 6a shows the adsorption spectra of RhB dye over the sample SA-6 measured at each 10 min time interval when exposed to UV illumination. As can be seen from the spectrum, the absorbance of RhB gradually decreases with the increasing the irradiation time. There is almost no adsorption after only 20 min photoreaction, indicating that the model dye has been completely decolorized. It has been widely accepted that hydroxyl radicals (OH•) play a key role during the process of photocatalytic degradation of dye molecules. We hence studied the formation of OH• on the surface of the sample SA-6 under UV irradiation by the PL-TA technique.[35] The formation of OH• on the surface of SA-6 was detected by the fluorescence technique using terephthalic acid (TA) as a probe molecule, which readily reacts with OH• to produce the highly fluorescent product, 2-hydroxyterephthalic acid (TAOH). Fig. 6b presents the fluorescence intensity of TAOH with an excitation source of 315 nm. It can be seen that the fluorescence intensity increases gradually with increasing irradiation time, indicating OH• is formed during this photocatalytic process under UV irradiation.

To compare the photocatalytic efficiency of different morphology and structure, we further performed photocatalytic experiments for the degradation of RhB in the presence of two previous reported fluorinated SnO_2 samples with excellent photocatalytic activities, i.e., fluorinated SnO_2 nanoparticles (sample NPs [7]) and hollow nanospheres (sample HSs [36]). Figure 7a displays the comparable photodegradation efficiencies of RhB of these samples. C_0 and C are the initial concentration after the equilibrium adsorption and the reaction concentration of the RhB, respectively. As can be seen, the degradation of RhB dye hardly occurs without the use of catalyst, while other solutions with SnO_2 nanocrystals added show significant photocatalytic degradation. In particular, the SA-6 presents much superior photocatalytic activity than any others. The inset shows the corresponding kinetic behavior of photocatalytic degradation. It can be seen that the constant κ (apparent first-order rate constant, could be obtained from the slope of the linear regression) for SA-6 (0.1319 min^{-1}) is about 1.34 and 2.05 times as much as that for HS (0.0981 min^{-1}) and NP (0.0642 min^{-1}) respectively. Further, the stability and durability of SA-6 was also tested. As can be seen from Figure 7b, after four cycle uses for photodegradation of RhB under the same conditions, the photocatalytic activity of SA-6 only has a loss of about 15%, indicating the sample SA-6 has a relative good stability and durability when used as photocatalyst.

It has been accepted that the practical performance of SnO_2 depends on its particle size, morphology, crystallinity, specific surface area, exposed facets and so on. In this case, as the surface area of SA-6 (61.5m^2/g) is found to be much smaller than that of the reported HS (134.3 m^2/g), the outstanding photocatalytic activity of SA-6 may be attributed to the fluorinated surface and the special hierarchical structure composed of ultrathin nanosheets. For one thing, the F ions

RSC Advances Accepted Manuscript

on the surface of SnO_2 nanosheets can reduce the recombination rate of photogenerated electrons and holes, and more important, promote the production of ·OH free radicals (which play a key role during the process of photocatalytic degradation of dye molecules) due to the replacement of fluoride with surface hydroxyl groups.[18, 23-25] For another, the excellent structure of SA-6 greatly benefits the photocatalysis. Firstly, the ultrathin nanosheets with large lateral size can offer more active sites and also enhance the efficiency of the electron-hole separation.[12-14] Second, according to the calculation results, the relative surface energies of SnO_2 crystals shows the sequence of (110) < (100) < (101) <(321) < (211) < (111) < (001) < (212) < (221) < (112).[37] The exposed $\{1\bar{1}1\}$ facets of the nanosheets have a higher relative surface energy, which can improve the photocatalytic activity. In addition, the 2D structure can adsorb more target molecules and incident light, and hence the photocatalysis efficiency can be enhanced.[15, 34]

4. Conclusions

In this paper, fluorinated SnO_2 hierarchical structures assembled from nanosheets were synthesized via a simple hydrothermal treatment of stannous fluoride in the presence of appropriate amount of adipic acid. The SnO_2 nanosheets with typical thickness of ~6nm showed pure tetragonal rutile structure. HRTEM image indicated that the SnO_2 nanosheets were single-crystalline nature and the exposed planes should be $\{1\bar{1}1\}$ facets. The surface area of the product was found to be 61.5m^2/g and a small amount of fluorine ions were observed to be adsorbed on the surface of SnO_2 physically. It was found that both of F^- and adipic acid played important roles in the formation of SnO_2 hierarchical nanostructures. The as-prepared SnO_2 nanosheets presented excellent photocatalytic degradation of RhB under UV light irradiation. When irradiated by a 300 W high-pressure mercury lamp, the degradation of RhB reached 100 % within 20 min. It is expected that the SnO_2 nanosheets will have potential commercial applications in the area of photocatalysis.

Acknowledgment

We gratefully acknowledge the financial support of the Key Program of Natural Science Foundation of Hubei Province (2015CFA129) and the National Natural Science Foundation of China (21477118).

Reference

1. X. C. Ma, H. Y. Song, C. H. Guan, *Sens. Actuators B*, 2013,**177**, 196.
2. H. K. Wang, K. P. Dou, W. Y. Teoh, Y. W. Zhan, T. F. Hung, F. H. Zhang, J. Q. Xu, R. Q. Zhang, A. L. Rogach, *Adv. Funct. Mater.*, 2013, **23**, 4847.
3. W. S. Kim, Y. Hwa, J. H. Jeun, H. J. Sohn, S. H. Hong, *J. Power Sources*, 2013, **225**, 108.
4. P. Gurunathan, P. M. Ette, K. Ramesha, *ACS Appl. Mater. Interfaces*, 2014, **6**, 16556.
5. Y. Masuda, T. Ohji, K. Kato, *ACS Appl. Mater. Interfaces*, 2012, **4**, 1666.
6. Y. Q. Zhu, H. Z. Guo, H. Z. Zhai, C. B. Cao, *ACS Appl. Mater. Interfaces*, 2015, **7**, 2745.
7. T. T. Hao, G. Cheng, H. Z. Ke, Y. J. Zhu, Y. M. Fu, *RSC Adv.*, 2014, **4**, 21548.
8. Y. Liu, Y. Jiao, Z. L. Zhang, F. Y. Qu, A. Umar, X. Wu, *ACS Appl. Mater. Interfaces*, 2014, **6**, 2174.
9. G. Wang, W. Lu, J. H. Li, J. Choi, Y. Jeong, S. Y. Choi, J. B. Park, M. K. Ryu, K. Lee, *small* 2006, **2**, 1436.
10. J. T. Park, C. S. Lee**,** J, H, Kim, *RSC Adv.*, 2014, **4**, 31452.
11. Y. Z. Wang, T. T. Su, H. Y. Chen, W. Liu, Y. G. Dong, S. L. Hu, *Mater. Lett.*, 2014,**137**, 241.
12. T. Oshima, D. Lu, O. Ishitani, K. Maeda, *Angew. Chem. Int. Ed.*, 2015, **54**, 2698.

RSC Advances Accepted Manuscript

13. B. Weng, X. Zhang, N. Zhang, Z. R. Tang, Y. J. Xu, *Langmuir*, 2015, **31**, 4314.
14. A. K. Singh, K. Mathew, H. L. Zhuang, R. G. Hennig, *J. Phys. Chem. Lett.*, 2015, **6**, 1087.
15. S. Ida, T. Ishihara, *J. Phys. Chem. Lett.*, 2014, **5**, 2533.
16. H. B. Wu, J. S. Chen, X. W. Lou, H. H. Hng, *J. Phys. Chem. C*, 2011, **115**, 24605.
17. H. G. Yang, C. H. Sun, S. Z. Qiao, J. Zou, G. Liu, S. C. Smith, H. M. Cheng, G. Q. Lu, *Nature*, 2008, **453**, 638.
18. H. G. Yang, G. Liu, S. Z. Qiao, C. H. Sun, Y. G. Jin, S. C. Smith, J. Zou, H. M. Cheng, G. Q. Lu, *J. Am. Chem. Soc.*, 2009, **131**, 4078.
19. J. Pan, G. Liu, G. Q. Lu, H. M. Cheng, *Angew. Chem. Int. Ed.*, 2011, **50**, 2133.
20. M. Liu, L. Y. Piao, L. Zhao, S. T. Ju, Z. J. Yan, T. He, C. L. Zhou, W. J. Wang, *Chem. Commun.*, 2010, **46**, 1664.
21. J. G. Yu, J. X. Low, W. Xiao, P. Zhou, M. Jaroniec, *J. Am. Chem. Soc.*, 2014, **136**, 8839.
22. J. S. Chen, M. F. Ng, H. B. Wu, L. Zhang, X. W. Lou, *CrystEngComm*, 2012, **14**, 5133.
23. C. Hu, X. Zhang, W. T. Li, Y. Yan, G. C. Xi, H. F. Yang, J. F. Li, H. Bai, *J. Mater. Chem. A*, 2014, **2**, 2040.
24. S. W. Liu, J. G. Yu, B. Cheng, M. Jaroniec, *Adv. Colloid Interface Sci.*, 2012, **173**, 35.
25. Y. F. Wang, L. P. Li, X. S. Huang, Q. Lia, G. S. Li, *RSC. Adv.,* 2015, **5**, 34302.
26. J. Fang, F. Wang, K. Qian, H. Z. Bao, Z. Q. Jiang, W. X. Huang, *J. Phys. Chem. C*, 2008, **112**, 18150.
27. J. G. Yu, S. W. Liu, M. H. Zhou, *J. Phys. Chem. C*, 2008, **112**, 2050.
28. Z. T. Deng, B. Peng, D. Chen, F. Q. Tang, A. J. Muscat, *Langmuir*, 2008, **24**, 11089.
29. Z. Tebby, T. Uddin, Y. Nicolas, C. Olivier, T. Toupance, C. Labrugère, L. Hirsch, *ACS. Appl. Mater. Interfaces*, 2011, **3**, 1485.
30. J. C. Yu, J. G. Yu, W. K. Ho, Z. T. Jiang, L. Z. Zhang, *Chem. Mater.*, 2002,**14**, 3808.
31. W. Jiao, L. Z. Wang, G. Liu, G. Q. Lu, H. M. Cheng, *ACS Catal.*, 2012, **2**, 1854.
32. X. Han, Q. Kuang, M. Jin, Z. X. Xie, L. S. Zheng, *J. Am. Chem. Soc.*, 2009, **131**,3152.
33. H. Ohgi, T. Maeda, E. Hosono, S. Fujihara, H. Imai, *Cryst. Growth Des.,* 2005, **3**, 1079.
34. W. J. Ong, L. L. Tan, S. P. Chai, S. T. Yong, A. R. Mohamed, *Nanoscale*, 2014, **6**, 1946.
35. S. Khanchandani, S. Kundu, A. Patra, A. K. Ganguli, *J. Phys. Chem. C*, 2013, **117**, 5558.
36. S. W. Liu, G. C. Huang, J. G. Yu, T. W. Ng, H. Y. Yip, P. K. Wong, *ACS Appl. Mater. Interfaces*, 2014, **6**, 2407.
37. B. Slater, C. R. A. Catlow, D. H. Gay, D. E. Williams,V. Dusastre, *J. Phys. Chem. B*, 1999**, 103**, 10644.

RSC Advances Accepted Manuscript

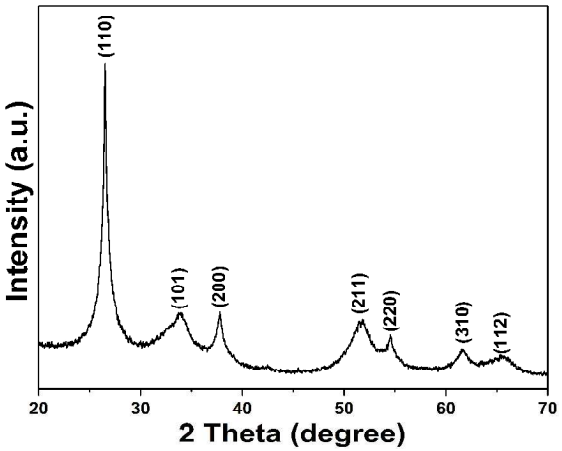

Fig.1 XRD pattern of **SA-6**

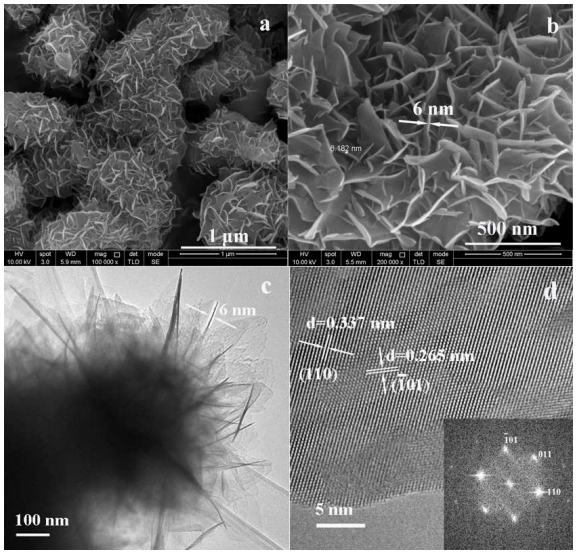

Fig.2 (a, b) SEM, (c) TEM and (d) HRTEM images of SA-6.

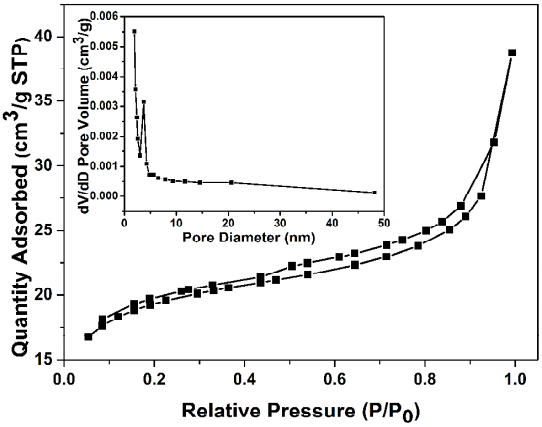

RSC Advances Accepted Manuscript

Fig.3 Nitrogen adsorption and desorption isotherms for SA-6. The inset showed the corresponding pore-size distribution.

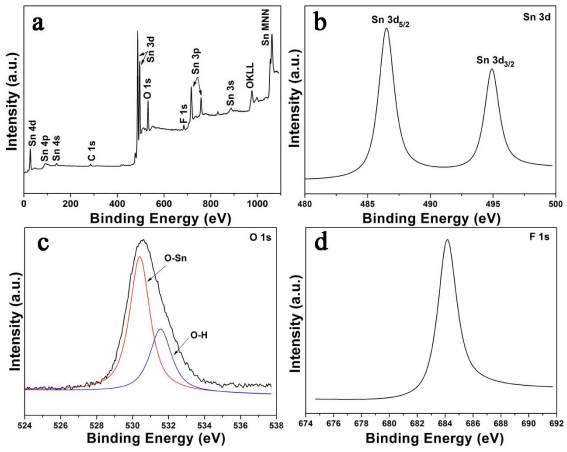

Fig.4 High-resolution XPS spectra of SA-6: (a) XPS full spectrum; (b) Sn 3d; (c) O 1s; (d) F 1s

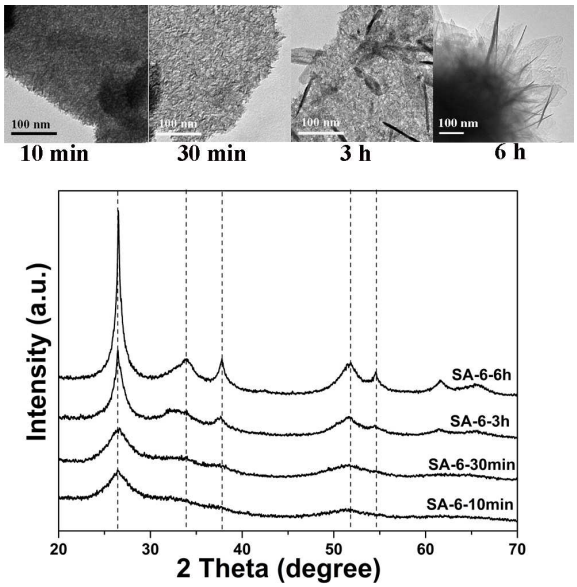

Fig.5 TEM images and XRD patterns of SA-6 collected at different hydrothermal time.

RSC Advances Accepted Manuscript

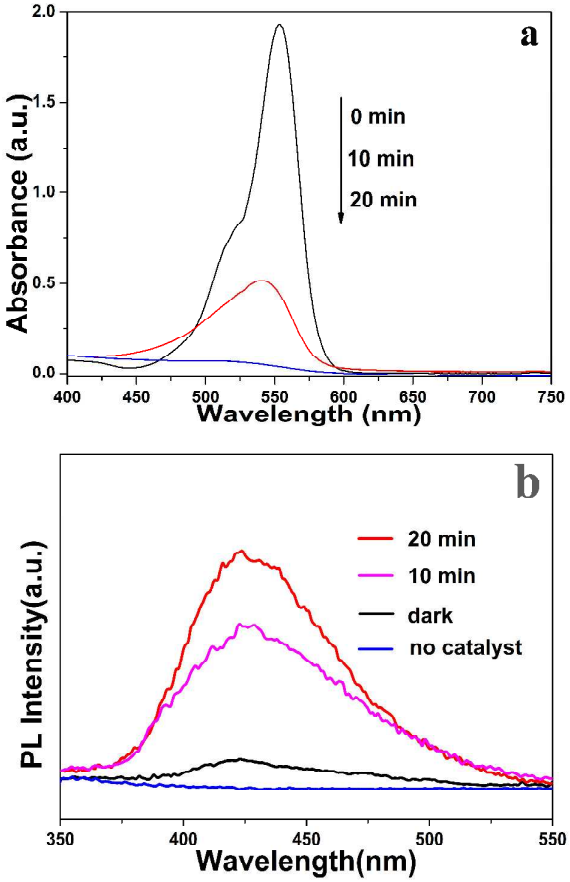

Fig.6 (a) Variations in adsorption spectra of RhB dye solution in the presence of SA-6 irradiated by a UV lamp for different time; (b) Fluorescence spectral changes measured during UV illumination of SA-6 in a solution of terephthalic acid.

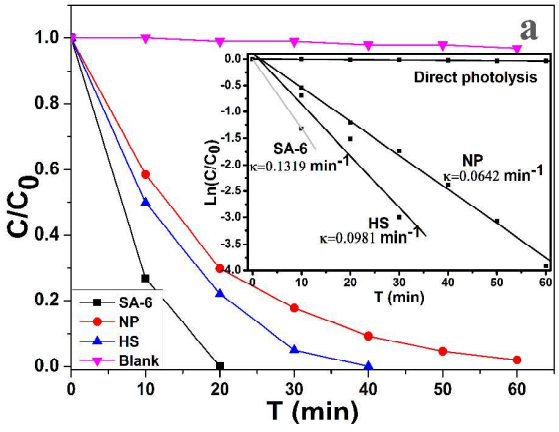

RSC Advances Accepted Manuscript

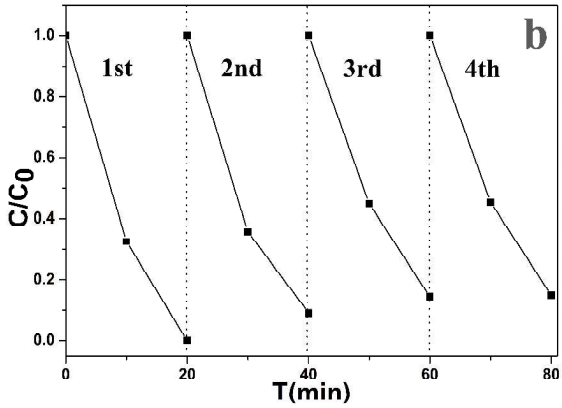

Fig.7 (a) Photocatalytic activities of prepared samples for degradation of RhB under UV irradiation (the inset shows $Ln(C/C_0)$ of RhB versus time for these samples under UV irradiation.); (b) Cycling runs in the photocatalytic degradation of RhB in the presence of SA-6 under UV irradiation.

RSC Advances Accepted Manuscript